Title	Geometric and Electronic Structures of Dibenzo-15-Crown-5 Complexes with Alkali Metal Ions Studied by UV Photodissociation and UV-UV Hole-Burning Spectroscopy
Auther(s)	Inokuchi, Yoshiya; Kida, Motoki; Ebata, Takayuki
Citation	Journal of Physical Chemistry A , 121 (5) : 954 - 962
Issue Date	2017-01-18
DOI	10.1021/acs.jpca.6b09653
Self DOI	
URL	http://ir.lib.hiroshima-u.ac.jp/00045932
Right	Copyright (c) 2017 American Chemical Society This document is the Accepted Manuscript version of a Published Work that appeared in final form in 'Journal of Physical Chemistry A', copyright © American Chemical Society after peer review and technical editing by the publisher. To access the final edited and published work see https://doi.org/10.1021/acs.jpca.6b09653. This is not the published version. Please cite only the published version. この論文は出版社版でありません。引用の際には出版社版をご確認ご利用ください。
Relation	


Hiroshima University Institutional Repository

Geometric and Electronic Structures of Dibenzo-15-Crown-5 Complexes with Alkali Metal Ions Studied by UV Photodissociation and UV-UV Hole-Burning Spectroscopy

Yoshiya Inokuchi,* Motoki Kida, and Takayuki Ebata

Department of Chemistry, Graduate School of Science, Hiroshima University, Higashi-Hiroshima, Hiroshima 739-8526, Japan

E-mail: y-inokuchi@hiroshima-u.ac.jp

Phone: +81 (Japan)-82-424-7101

Abstract

We measure UV photodissociation (UVPD) and UV-UV hole-burning (HB) spectra of dibenzo-15-crown-5 (DB15C5) complexes with alkali metal ions, M^+•DB15C5 (M = Li, Na, K, Rb, and Cs), under cold (~10 K) conditions in the gas phase. The UV-UV HB spectra of the M^+•DB15C5 (M = K, Rb, and Cs) complexes indicate that there is one dominant conformation for each complex except the Na^+•DB15C5 complex, which has two conformers with a comparable abundance ratio. It was previously reported that the M^+•(benzo-15-crown-5) (M^+•B15C5, M = K, Rb, and Cs) complexes each have three conformers. Thus, the attachment of one additional benzene ring to the crown cavity of benzo-15-crown-5 reduces conformational flexibility, giving one dominant conformation for the M^+•DB15C5 (M = K, Rb, and Cs) complexes. In the UVPD spectra of the K^+•DB15C5, Rb^+•DB15C5, and Cs^+•DB15C5 complexes, the S_1–S_0 and S_2–S_0 transitions are observed independently at different

positions with different vibronic structures. The spectral features are substantially different from those of the K^+•(dibenzo-18-crown-6) (K^+•DB18C6) complex, which belongs to C_{2v} point group and exhibits the exciton splitting with an interval of 2.7 cm^{-1}. The experimental and theoretical results suggest that in the M^+•DB15C5 complexes the two benzene rings are not symmetrically equivalent with each other, and the S_1–S_0 and S_2–S_0 electronic excitations are almost localized in one of the benzene rings. The electronic interaction energy between the two benzene chromophores is compared between the K^+•DB15C5 and K^+•DB18C6 complexes by quantum chemical calculations. The interaction energy of the K^+•DB15C5 complex is estimated to be less than a half of the K^+•DB18C6 complex (~30 cm^{-1}) due to less suitable relative angles between the transition dipole moments of the two benzene chromophores in K^+•DB15C5.

*To whom correspondence should be addressed.

1. INTRODUCTION

Crown ethers (CEs) have been widely used as host molecules in host-guest, supramolecular, and organic chemistry.[1-2] One of the characteristics of CEs is the ion selectivity in solution.[3] Efficient and preferential capture of guest species by CEs will be driven by conformational flexibility; the bigger the number of conformations is, the more favorable the complex formation is, and flexible cavities of CEs can maximize the intermolecular interaction with guest species. Determination of the structure for guest ion–CE complexes has been extensively done by X-ray diffraction analysis of crystals. However, reports on X-ray diffraction analysis tend to be limited to optimum or selective systems, because non-optimum systems hardly form stable crystals.[4] In addition, X-ray analysis may not be suitable for searching whole conformational landscapes, because the complex conformation is confined by crystal fields. From this standpoint, gas-phase spectroscopic studies of CEs will play a vital role in the elucidation for the ion selectivity of CEs in solution.[5-24] Since the structure of CE complexes in the gas phase is not perturbed either by neighboring complexes, counteranions, or solvent molecules, the gas-phase spectroscopy will shed light on intrinsic natures of the conformation.

In this study, we measure UV photodissociation (UVPD) spectra of dibenzo-15-crown-5 (DB15C5, Scheme 1) complexes with alkali metal ions, M^+•DB15C5 (M = Li, Na, K, Rb, and Cs), under cold gas-phase conditions. We apply UV-UV hole-burning (HB) spectroscopy to the M^+•DB15C5 complexes for discriminating vibronic bands of a single isomer. The number and structure of isomers are determined on the basis of the results of UVPD and UV-UV HB experiments with the aid of quantum chemical calculations. We will compare the geometric and

electronic structures and the number of isomers between the metal ion complexes of DB15C5, benzo-15-crown-5 (B15C5), and dibenzo-18-crown-6 (DB18C6) to examine the effect of a phenyl ring to the conformational flexibility and of the crown size to the electronic structure.

2. EXPERIMENTAL AND COMPUTATIONAL METHODS

Details of the experiment for UVPD and UV-UV HB spectroscopy have been described in our previous papers.[24-25] Briefly, the M^+•DB15C5 (M = Li, Na, K, Rb, and Cs) complexes are produced by electrospray ion source with methanol solutions of MCl salt and DB15C5 with a concentration of ~100 μM each, and introduced into a cold, Paul-type quadrupoe ion trap (QIT). The QIT is cooled to ~4 K by a He cryostat, and He buffer gas is continuously introduced into the QIT. The ions are stored in the QIT for ~90 ms and cooled translationally and internally by the collision with the cold He buffer gas. We estimated the vibrational temperature of trapped ions as ~10 K from the intensity of a hot band in the UVPD spectrum of K^+•(benzo-18-crown-6) (K^+•B18C6) complex.[25] Ions other than parent ions of interest can be removed from the QIT by an RF potential applied to the entrance end cap, as was done by Kang et al.[26] The M^+•DB15C5 ions are then irradiated by a UV laser, and resulting fragment M^+ ions are mass-analyzed and detected with a home-made time-of-flight mass spectrometer.[27] The UVPD spectra are obtained by plotting yields of the fragment ions against the wavenumber of the UV laser. In the UV-UV HB experiments of the M^+•DB15C5 (M = K, Rb, and Cs) complexes, we use two UV laser systems for the pump and probe light. The pump laser is introduced to the QIT prior to the probe one by 10–100 μs. In the case of the K^+•DB15C5 complex, the fragment K^+ ion produced by the pump laser is removed by the RF field applied to the ring electrode of the QIT. For the

Rb^+•DB15C5 and Cs^+•DB15C5 complexes, the fragment Rb^+ and Cs^+ ions due to the pump laser are ejected by an additional RF potential applied to the entrance end cap.[26] The wavenumber of the pump laser is scanned while that of the probe laser is fixed to a position of a vibronic band. The UV-UV HB spectra are obtained by plotting the ratio of the fragment ion intensity with the pump laser on/off (I_{on}/I_{off}) as a function of the wavenumber of the pump laser.[24]

We also perform quantum chemical calculations for the M^+•DB15C5 complexes. The initial conformation search is performed with the CONFLEX High Performance Conformation Analysis program with the MMFF94s force field for the Li^+•DB15C5, Na^+•DB15C5, and K^+•DB15C5 complexes.[21, 28-30] The structure of conformers obtained by the initial search is further optimized with the GAUSSIAN09 program package at the M05-2X/6-31+G(d) level of theory; at least 10 conformers are calculated for the M^+•DB15C5 complexes each.[31] The vibrational analysis is also performed at the same calculation level. The transition energies and the oscillator strengths are obtained by time-dependent density functional theory (TD-DFT) calculations at the M05-2X/6-31+G(d) level. For comparison of calculated UV spectra with the UVPD spectra, a scaling factor of 0.8340 is employed for the calculated transition energy at the M05-2X/6-31+G(d) level. This factor was determined so as to reproduce the transition energy of the K^+•DB18C6 complex, and it was applicable very well to alkali metal ion complexes of DB18C6, B18C6, B15C5, and benzo-12-crown-4 (B12C4).[18-19, 24] For the Rb^+•DB15C5 and Cs^+•DB15C5 complexes, the initial structure for the geometry optimization with the GAUSSIAN09 is obtained by replacing the K^+ ion in the stable conformers of the K^+•DB15C5 complex with Rb^+ or Cs^+ ion. For Rb and Cs, we use the Stuttgart RLC as effective core potentials (ECPs). Functions of the

ECPs are obtained from a database of basis sets,[32] and they provided quite reasonable results in our previous papers of CE ion complexes.[18-19, 24]

3. RESULTS AND DISCUSSION

3.1. UV Photodissociation Spectra

Figure 1 displays the UVPD spectra of the M^+•DB15C5 (M = Li, Na, K, Rb, and Cs) complexes in the 36000–37500 cm^{-1} region. Thanks to the cooling of the ions in the QIT,[25] the complexes of the K^+, Rb^+, and Cs^+ ions show sharp and well-resolved vibronic bands (Figs. 1c–e). The UVPD spectrum of the K^+•DB15C5 complex (Fig. 1c) has an extensive and intense progression in the 36600–36800 cm^{-1} region with an interval of 22 cm^{-1}, but with no strong origin band. In addition to this progression, a strong band also appears at 36839 cm^{-1}, followed by a progression of several vibronic bands with an interval of ~26 cm^{-1}. Since the interval and intensity pattern are different between these two progressions, these can be ascribed to different isomers or different electronic states. These low-frequency progressions are due to torsional motions of the ether ring; similar low-frequency progressions were observed for the M^+•DB18C6 complexes.[18] In the case of the M^+•B15C5 (M = K, Rb, and Cs) complexes, three vibronic structures appear in each of their UVPD spectra, and these were assigned to three different conformers with IR spectroscopy.[19] The Rb^+•DB15C5 and Cs^+•DB15C5 complexes show similar spectral features (Figs. 1d and e) to those of K^+•DB15C5; a strong band is observed at 36810 and 36768 cm^{-1}, accompanied by several vibronic bands on the higher frequency side, and an extensive progression on the lower frequency side. In addition to these strong bands, the M^+•DB15C5 (M = K, Rb, and Cs) complexes have very weak, well-resolved bands in the 36200–36500 cm^{-1} region, as shown in inset of Figs. 1c–e. The relative intensity of these bands to the

main components around 36800 cm^{-1} becomes stronger with decreasing the ion size from Cs^+ to K^+. The spectral pattern of the Na^+•DB15C5 complex (Fig. 1b) seems to be similar to that of the K^+ complex. The absorption above 36600 cm^{-1} shows broader features with a few resolved bands, and the low-frequency component in the 36300–36600 cm^{-1} region becomes stronger than the case of the K^+ complex. The UVPD spectrum of the Li^+ complex (Fig. 1a) has congested features around 36750 cm^{-1} with a smaller signal to noise ratio than that of the other complexes.

3.2. UV-UV Hole-Burning Spectra

For discriminating bands of different conformers in the UVPD spectra, we perform UV-UV HB spectroscopy to the K^+, Rb^+, and Cs^+ complexes. Figure 2 displays the UV-UV HB spectra (red and blue curves) with the UVPD spectra (black curves) for the M^+•DB15C5 (M = K, Rb, and Cs) complexes. It was not possible to measure UV-UV HB spectra for the Na^+ and Li^+ complexes because of their smaller photodissociation efficiency. The red spectra in Figs. 2a–c are measured by fixing the probe laser frequencies to the strong bands at 36839, 36810, and 36768 cm^{-1} for the K^+, Rb^+, and Cs^+ complexes, respectively. The positions of the probe laser are shown with red arrows in the UVPD spectra of Fig. 2. The UV-UV HB spectra seem to be saturated and the relative intensity of the vibronic bands is different between the UVPD and the UV-UV HB spectra, but all the vibronic bands, which include the extensive progression on the lower frequency side, appear in the UV-UV HB spectra. For the K^+ and Rb^+ complexes, UV-UV HB spectra are also measured by probing one of the extensive progressions at 36765 and 36685 cm^{-1}, respectively (blue curves in Figs. 2a and b); the probe positions are shown with blue arrows in Figs. 2a and b. The blue spectra in Figs. 2a and b also show all the vibronic bands in the UVPD spectra. These

HB results indicate that all the vibronic bands appearing in the 36500–37000 cm^{-1} region are due to a single isomer. Hence, the two progressions in the UVPD spectra can be assigned to the S_1–S_0 and S_2–S_0 transitions of the single isomer. For the K^+•DB15C5 complex, we extend the measurement region of UV-UV HB spectroscopy up to 36200 cm^{-1} (Fig. 2d) with the probe position of 36839 cm^{-1} to see if the weak absorption in the 36200–36500 cm^{-1} region is due to the same conformer. Since the HB spectrum colored in red in Fig. 2d does not show any noticeable depletion in the 36200–36500 cm^{-1} region, the weak components of the M^+•DB15C5 (M = K, Rb, and Cs) complexes in the 36200–36500 region are assigned to a less stable, another isomer.

3.3. Geometric Structure of the M^+•DB15C5 Complexes

The geometric structure of the M^+•DB15C5 complexes can be determined on the basis of the UVPD and UV-UV HB results with the aid of quantum chemical calculations. Figure 3 shows the most (a–e) and the second most (f–j) stable isomers of the M^+•DB15C5 (M = Li, Na, K, Rb, and Cs) complexes. The numbers in the figure present the dihedral angles in degrees around the benzene rings: C15–O1–C2–C16, C5–O4–C3–C19, C6–O7–C8–C20, and C11–O10–C9–C23 (the atom numbering see Scheme 1). The structure in Fig. 3 indicates that the difference of the isomers of each species is the conformation of the DB15C5 part. As seen in Figs. 2a–c, the main component in the UV spectra of the K^+, Rb^+, and Cs^+ complexes can be assigned to a substantially stable, single conformer. Since the spectral features in the UVPD spectra are similar for the K^+, Rb^+, and Cs^+ complexes (Figs. 1c–e), the geometric structure of the main conformers will be similar for these complexes. These experimental results described above well coincide with the trend of calculated total energies and structures. The energy difference between the most and the second most stable conformers is quite

large: 4.5, 5.6, and 6.1 kJ/mol for the K^+, Rb^+, and Cs^+ complexes, respectively (see Figs. 3h–j), suggesting that one quite stable conformer exists for each of these complexes under cold experimental conditions. In addition, the most stable conformers (K-A, Rb-A, and Cs-A in Fig. 3) have similar conformations; the difference in the dihedral angles shown in Figs. 3c–e is less than 6 degrees. Hence, the main component in the UVPD spectra of the M^+•DB15C5 (M = K, Rb, and Cs) complexes can be attributed to the most stable conformers (K-A, Rb-A, and Cs-A in Fig. 3). It should be noted that in all the M^+•DB15C5 conformers the two benzene chromophores are not symmetrically equivalent with each other. This makes characteristic features in the electronic spectra of the complexes as will be discussed later.

The weak absorption of the M^+•DB15C5 (M = K, Rb, and Cs) complexes in the 36200–36500 cm^{-1} region can be attributed to the second most stable conformers (K-B, Rb-B, and Cs-B in Fig. 3) based on the total energy and the calculated electronic transitions. Figure 4 displays the comparison of the UVPD spectra with the results of the TD-DFT calculations (red and blue bars) for the M^+•DB15C5 complexes. The red and blue bars correspond to electronic transitions of the most and the second most stable conformers, respectively. There are two transitions, S_1–S_0 and S_2–S_0, for each conformer in this region; these originate from the two benzene rings. As seen in Figs. 4c–e, the TD-DFT calculations for the most stable conformers (K-A, Rb-A, and Cs-A) well reproduce the position of the main absorption in the UVPD spectra around 36700 cm^{-1}. This supports the assignment of the main absorption in the UVPD spectra to the most stable conformers. The electronic transition of the second most stable conformers (K-B, Rb-B, and Cs-B) is located on the lower energy side of that of the most stable ones, which coincides with the relative position of the weak absorption against the strong one at ~36700 cm^{-1} in the UVPD spectra. In addition, the difference

in the total energy between the most and the second most stable conformers in S_0 becomes smaller and smaller with decreasing the ion size from Cs^+ (6.1 kJ/mol) to K^+ (4.5 kJ/mol). This trend in the total energy agrees with the increase of the relative intensity of the weak component from the Cs^+ to K^+ complex as seen in Fig. 1.

In the case of the Na^+•DB15C5 complex, it is possible to assign the UVPD spectrum and determine the structure on the basis of the spectral similarity with the K^+•DB15C5 complex. The most and second most stable conformers of the Na^+•DB15C5 complex are shown in Figs. 3b and g, respectively. It should be noted that the conformation of Na-A and Na-B is similar to that of K-B and K-A, respectively. This indicates that the switching of the stability for the two most stable conformers occurs between Na and K. The difference in the total energy between Na-A and Na-B is only 0.5 kJ/mol, suggesting the possibility of noticeable coexistence for these conformers in the experiment. Similar to the case of K-A and K-B, the electronic transition of Na-A is located on the lower frequency side of that of Na-B, as seen in Fig. 4b. Hence, we can assign the lower-frequency component in the 36300–36600 cm^{-1} region to Na-A, and the absorption above ~36600 cm^{-1} is ascribed to Na-B. For the Li^+ complex, the most stable form (Li-A in Fig. 3) well reproduces the position of the absorption as seen in Fig. 4a. In addition, the difference in the total energy between the most (Li-A) and the second most (Li-B) stable conformers is fairly large (3.1 kJ/mol). Hence, we tentatively assign the structure of the Li^+•DB15C5 complex to Li-A in Fig. 3a.

3.4. Conformational Flexibility of the M^+•DB15C5 and M^+•B15C5 Complexes

The geometric and electronic structures are in marked contrast between the M^+•DB15C5, M^+•B15C5, and M^+•DB18C6 complexes. Figure 5 shows the UVPD

spectra of the K^+•DB15C5, K^+•B15C5, and K^+•DB18C6 complexes.[18-19] The labeling of the conformations for the B15C5 (K-C, K-B, and K-E) and DB18C6 (K-a) complexes is the same as that used in our previous papers.[18-19] Table 1 presents the number of conformers experimentally determined for the M^+•DB15C5, M^+•B15C5, and M^+•DB18C6 complexes under cold conditions.[18-19] As described above, the UVPD spectrum of the K^+•DB15C5 complex (Fig. 5a) is assigned to the S_1–S_0 and S_2–S_0 transitions of the most stable conformer (K-A). The K^+•B15C5 complex shows three different vibronic structures in the UVPD spectrum. From the results of IR-UV double-resonance spectroscopy, we assigned them to three different conformers (K-C, K-B, and K-E in Fig. 5b).[19] Substitution of a part of a crown cavity with a benzene ring forces the crown ring to a planar form because of the delocalization of the π cloud to neighboring oxygen atoms. For example, neutral 1,2-dimethoxybenzene has a planar form with the oxygen and carbon atoms of the methoxy groups and the benzene plane.[33-34] The attachment of one additional phenyl group to B15C5 reduces conformation flexibility, giving one dominant conformer for K^+•DB15C5. The reduction of the conformation number occurs also for the M^+•B18C6 and M^+•DB18C6 complexes.[19] Hence, the result of the reduction for M^+•DB15C5 along with that for M^+•DB18C6 reinforces the conclusion that the phenyl ring in the crown cavity reduces the crown flexibility in the metal ion complexes.

3.5. Electronic Interaction in the M^+•DB15C5 and M^+•DB18C6 Complexes

It was reported that the K^+•DB18C6 complex has only one conformer (K-a in Fig. 5c) under cold gas-phase conditions,[18] the same as the case of K^+•DB15C5, but the electronic spectrum is substantially different between K^+•DB18C6 and K^+•DB15C5. These complexes have two benzene chromophores and they interact with each other.

In the UVPD spectrum of the K^+•DB18C6 complex, the interaction appears as an exciton splitting for vibronic bands with an interval of 2.7 cm^{-1}.[18] This complex belongs to C_{2v} point group and two benzene rings are symmetrically equivalent. In contrast, in the spectrum of the K^+•DB15C5 complex the S_1–S_0 and S_2–S_0 transitions are separated by more than 100 cm^{-1} with quite different vibronic structures; the S_1–S_0 transition shows an intense and extensive progression, while the S_2–S_0 transition has a strong origin band followed by several vibronic bands. The large separation of the electronic transitions and different vibronic structures will be due to the fact that the two benzene rings are symmetrically inequivalent in K^+•DB15C5 as shown in Fig. 3.

Figure 6 presents molecular orbitals (MOs) that contribute the most to the S_1–S_0 and S_2–S_0 transitions of the K^+•DB15C5 (K-A) and K^+•DB18C6 (K-a) complexes. Interestingly, the MOs and resulting electronic transitions are almost localized in one of the two benzene rings for the K^+•DB15C5 complex (Fig. 6a); the electronic interaction between the two benzene rings is quite small. In contrast, the K^+•DB18C6 complex (K-a) belongs to C_{2v} point group, and as a result the MOs are equally distributed to the two benzene rings. For the K^+•DB18C6 complex (K-a), the distance between the centers of the benzene rings is 9.1 Å. In the case of the K^+•DB15C5 complex (K-A), the distance is 8.0 Å, slightly shorter than that of K^+•DB18C6. In spite of the shorter distance, the electronic interaction between the benzene rings seems to be very weak for K^+•DB15C5. Hence, it is probable that the main reason for very weak electronic interaction in the K^+•DB15C5 complex is a substantially large difference in the electronic transition energy of the two benzene rings due to their inequivalent natures. In addition, it is also plausible that the relative configuration of the benzene rings is not suitable very much for the interaction in the K^+•DB15C5 complex. Conformer-dependent interactions between the two benzene chromophores were also

found in DB18C6 and H_2O•DB18C6 complex, where a boat-type DB18C6 conformer shows a 5 cm^{-1} exciton splitting, while other conformers in which two chromophores are symmetrically inequivalent show separated electronic transitions.[11]

It would be intriguing to compare the results of the dibenzo-CE complexes described above with those of aromatic dimers, which show excitonic interactions between the two aromatic chromophores. The excitonic splitting has been studied experimentally and theoretically for aromatic molecular clusters in the gas phase.[35-37] Leutwyler and co-workers have extensively investigated the excitonic splitting of aromatic dimers by UV spectroscopy and ab initio calculations.[38-48] In their recent review, excitonic interactions were classified into three categories on the basis of coupling strength (Table 1 of Ref. 47): strong, weak, and very weak interactions.[47] As described later, the K^+•DB15C5 and K^+•DB18C6 complexes can be assigned to the "very weak" and "weak" groups, respectively. For the dibenzo-CE systems, the excited states can be expressed by linear combinations of ϕ_a^*• ϕ_b and ϕ_a• ϕ_b^*:

$$\Psi_+ = \alpha\bullet\phi_a^*\bullet\ \phi_b + \beta\bullet\phi_a\bullet\ \phi_b^* \qquad (1a)$$

$$\Psi_- = \beta\bullet\phi_a^*\bullet\ \phi_b - \alpha\bullet\phi_a\bullet\ \phi_b^* \qquad (1b)$$

where $\phi_{a(b)}^*$ and $\phi_{a(b)}$ are wavefunctions of two chromophores (a and b) in the S_1 and S_0 states, respectively. In order to estimate the electronic excitonic interaction energy of the K^+•DB15C5 and K^+•DB18C6 complexes, we compare the S_1–S_0 and S_2–S_0 electronic transition energies of the complexes with the S_1–S_0 transition energy of the chromophores. The right part of Figure 7 shows the calculated electronic transition energies of the K^+•DB18C6 (a) and K^+•DB15C5 (b) complexes. We calculate the S_1–S_0 electronic transition energy of the chromophores in the complexes by keeping the

structure of the most stable conformers (Fig. 6) and replacing one of the benzene rings ($-C_6H_4-$) with a –CH=CH– component. The results of the chromophores are shown in the left part of Figure 7. In the case of the K^+•DB18C6 complex (Fig. 7a), the S_1 energy levels of the two chromophores are degenerate since they are completely equivalent in the C_{2v} form of K^+•DB18C6. The S_1 levels of the chromophores are located right in the middle between the S_1 and S_2 states of the K^+•DB18C6 complex. The excitonic interaction energy can be estimated as ~27 cm^{-1}, as seen in Fig. 7a (a half of 55 cm^{-1}). For the K^+•DB15C5 complex (Fig. 7b), the difference in the S_1–S_0 transition energy of the two chromophores is calculated to be 63 cm^{-1}. The S_1–S_2 energy gap of the complex (66 cm^{-1}) is mostly due to the difference in the S_1–S_0 electronic transition energy between the two inequivalent chromophores. The interaction energy is estimated to be 10 cm^{-1} from the difference in the S_1–S_0 transition energy of the two chromophores (63 cm^{-1}) and the S_1–S_2 gap of the complex (66 cm^{-1}) (see the Supporting Information). The interaction energy in K^+•DB15C5 (10 cm^{-1}) is substantially smaller than that of K^+•DB18C6 (27 cm^{-1}). These results based on the TD-DFT calculations are consistent with the conclusion derived from the MOs of the complexes in Fig. 6 that the electronic interaction between the two benzene rings is quite small in the K^+•DB15C5 complex.

We estimate the electronic excitonic interaction energy also with the transition dipole moments of the two chromophores. In the weak interaction model, the S_1–S_2 splitting energy of vibronic transitions (ΔE) for systems having two equivalent chromophores is given by the following equations:

$$\Delta E = 2 \bullet F \bullet V_{ab} \qquad (2)$$

$$V_{ab} = |\boldsymbol{\mu}_a| \bullet |\boldsymbol{\mu}_b| \bullet (4\pi\varepsilon_0 R_{ab}^{\ 3})^{-1} \bullet (2\cos\theta_a \bullet \cos\theta_b - \sin\theta_a \bullet \sin\theta_b \bullet \cos\phi) \qquad (3)$$

where $\boldsymbol{\mu}_a$ and $\boldsymbol{\mu}_b$ are the transition dipole moments of the two chromophores, R_{ab} is the distance between the two chromophores, θ_a and θ_b are the angles of the transition dipole moments to the line connecting the two chromophores, and ϕ is the dihedral angle between $\boldsymbol{\mu}_a$ and $\boldsymbol{\mu}_b$.[8, 35, 38, 47-48] V_{ab} represents the electronic part, corresponding to the electronic interaction energy estimated above, and F is the vibrational part, which takes the Franck-Condon factor into account. We estimate the V_{ab} value of the K^+•DB15C5 and K^+•DB18C6 complexes by using equation (3), the geometry of the most stable conformers (Fig. 6), and the calculated transition dipole moments of the two chromophores described above. Table 2 collects $|\boldsymbol{\mu}_a|$, $|\boldsymbol{\mu}_b|$, R_{ab}, the energy part of equation (3), and the estimated V_{ab} values. The transition dipole moments of the two chromophores are almost parallel to the benzene plane and perpendicular to benzene C–C bonds forming the ether ring, such as C2–C3 and C11–C12 of DB18C6 (see Scheme 1). For the K^+•DB18C6 complex, we obtain V_{ab} = 33 cm^{-1} with equation (3). This value agrees with the interaction energy (27 cm^{-1}) obtained with the calculated energies of the electronic states (Fig. 7). In the case of the K^+•DB15C5 complex, as supposed from the geometry of the complex, the energy part of equation (3) (17 cm^{-1}, see the third column from the right in Table 2) is almost the same as that of the K^+•DB18C6 complex (18 cm^{-1}). However, since the angle part of the DB15C5 complex is fairly smaller than that of the DB18C6 one, the V_{ab} value of the K^+•DB15C5 complex (17 cm^{-1}) is much smaller than that of K^+•DB18C6 (33 cm^{-1}), which agrees with the trend of the TD-DFT results described above or in the rightmost column of Table 2. Hence, the main reason of very weak electronic interaction in the K^+•DB15C5 complex is its less suitable arrangement (not distance but relative angles) of the two benzene rings than that of the K^+•DB18C6 complex.

In order to examine the degree of localization for the electronic transitions of the K^+•DB15C5 complex quantitatively, we estimate the contribution (%) of the electronic transition on each benzene ring to the S_1–S_0 and S_2–S_0 transitions of the K^+•DB15C5 complex (Table 3). These values are estimated by two ways. One is based on the calculated S_1–S_0 and S_2–S_0 transition energies of the complexes and the calculated S_1–S_0 transition energy of the two chromophores; the contribution corresponds to the square of coefficients α and β in equation (1). In the other, the contribution is estimated from the results of the TD-DFT calculations. The calculations provide coefficients for electron promotion between two MOs for the electronic transitions of the complexes. Hence, we can estimate the contribution of each chromophore to the electronic transitions of the complexes from these coefficients. It is quite obvious in Table 3 that the S_1–S_0 and S_2–S_0 transitions of the K^+•DB15C5 complex are localized in one of the two benzene rings. In addition, the UVPD spectrum of the K^+•DB15C5 complex in the present study shows separated S_1 and S_2 excited states. The vibronic structures of the S_1–S_0 and S_2–S_0 transitions of the K^+•DB15C5 complex are quite different from each other; the S_1–S_0 transition shows an intense and extensive progression, whereas the S_2–S_0 transition has a strong origin band followed by several vibronic bands. These theoretical and experimental results strongly suggest that the K^+•DB15C5 complex has no or very weak excitonic interaction between the benzene rings, different from the case of the K^+•DB18C6 complex.[18] This conclusion indicates that the K^+•DB15C5 complex belongs to the "very weak" category of excitonic interactions.[47]

As mentioned in the studies of excitonic interactions done by Leutwyler and co-workers, in symmetric, planar aromatic dimers with inversion symmetry, the

out-of-phase combination of the transition dipole moments of the two chromophores is forbidden.[47] However, the vibronic coupling between the electronic excited state and asymmetric vibrations breaks the symmetry, giving a double-minimum potential energy surface along asymmetric vibrations. This results in localized vibronic transitions and the exciton splitting in UV spectra. Therefore, the observation of the exciton splitting for the aromatic dimers is a definitive evidence of "weak" excitonic interactions and the existence of the vibronic coupling. The magnitude of the excitonic splitting depends mainly on the height of the potential energy barrier and distance between the two minima.[47-48] In contrast, the situation of the K^+•DB18C6 complex is slightly different from the case of the planar aromatic dimers. The K^+•DB18C6 complex has a non-planar, C_{2v} structure. The transition dipole moments of the two benzene rings are parallel to the benzene ring, and are perpendicular to the C2–C3 and C11–C12 bonds (see Scheme 1 and Fig. 7a). As a result, both the in-phase and our-of-phase combinations of the two transition dipole moments are allowed, different from the case of the planar aromatic dimers.[47] Hence, it is not so obvious that the exciton splitting found for the K^+•DB18C6 complex is due to the vibronic coupling.[47] However, as mentioned above, the interaction energy of the K^+•DB18C6 complex is estimated as ~30 cm^{-1}, which is substantially larger than the exciton splitting (2.7 cm^{-1}) observed in the UVPD spectrum.[18] As Leutwyler and co-workers pointed out, the vibronic coupling provides not only the exciton splitting of vibronic bands but a considerable reduction of the electronic excitonic splitting in weak coupling case, which corresponds to coefficient F in equation (2).[47] Hence, a reduction of the electronic excitonic splitting due to the vibronic coupling occurs also for the K^+•DB18C6 complex.[47] For the K^+•DB18C6 complex, the vibrational part F can be estimated as F = ~0.05 from the value of V_{ab} = ~30 cm^{-1} in Table 2 and the exciton splitting ($2 \bullet F \bullet V_{ab}$ = 2.7 cm^{-1})

observed for vibronic transitions of the K^+•DB18C6 complex.[18] This value is similar to that of neutral DB18C6 (F = ~0.1).[8] As was done by Leutwyler, Köppel, and their co-workers,[37, 47] precise, high-level theoretical treatments including both the excitonic interaction and the vibronic coupling will be necessary to shed light on details of the electronic interaction in the metal ion–benzo-CE complexes, which will be our future work. These calculations will separate electronic and vibrational wavefunctions in the vibronic coupling of the K^+•DB18C6 complex and provide concrete physical insights into the exciton splitting and vibrations that give a double-minimum potential.

4. SUMMARY

The UVPD spectra of the M^+•DB15C5 (M = Li, Na, K, Rb, and Cs) complexes have been measured in the 36000–37500 cm^{-1} region under cold conditions (~10 K) in the gas phase. The M^+•DB15C5 (M = K, Rb, and Cs) complexes show sharp vibronic bands in this region. The UV-UV HB spectra have been measured for these complexes, and one dominant isomer was found for each of the M^+•DB15C5 (M = K, Rb, and Cs) complexes, in addition to a minor one, which shows weak absorption in the 36200–36500 cm^{-1} region. For the Na^+•DB15C5 complex, there are two isomers and they give absorption with comparable intensity in the UVPD spectrum. The two progressions emerging in the UVPD spectra of the M^+•DB15C5 (M = K, Rb, and Cs) complexes are assigned to the S_1–S_0 and S_2–S_0 transitions of the most stable conformers (K-A, Rb-A, and Cs-A in Fig. 3). In the case of the K^+•B15C5 complexes, there are three stable conformers. The attachment of one additional benzene ring to B15C5 reduces the conformational flexibility and the number of conformers from three to one for the K^+•DB15C5 complexes. For the K^+•DB15C5 complexes, the S_1–S_0 and S_2–S_0 transitions are almost localized in one of the two benzene rings. These experimental

and theoretical results suggest that the environment of the two benzene rings is quite different in the M^+•DB15C5 (M = K, Rb, and Cs) complexes. We estimated the electronic excitonic interaction energy between the benzene rings state for the K^+•DB15C5 and K^+•DB18C6 complexes by using the results of the DFT and TD-DFT calculations. The interaction energy of the K^+•DB18C6 complex is ~30 cm^{-1}, while that of the K^+•DB15C5 complex is less than a half of the K^+•DB18C6 value. The main reason of weaker interaction in the K^+•DB15C5 complex is its less suitable arrangement of the two benzene rings than that of the K^+•DB18C6 complex.

Acknowledgment

This work was partly supported by JSPS KAKENHI Grant Number 16H04098.

Supporting Information Available: Calculation of the interaction energy and full list of authors of Ref. 31. This material is available free of charge *via* the internet at http://pubs.acs.org.

References

(1) Pedersen, C. J. Cyclic Polyethers and Their Complexes with Metal Salts. *J. Am. Chem. Soc.* **1967**, *89*, 7017-7036.

(2) Pedersen, C. J. The Discovery of Crown Ethers. *Science* **1988**, *241*, 536-540.

(3) Izatt, R. M.; Bradshaw, J. S.; Nielsen, S. A.; Lamb, J. D.; Christensen, J. J. Thermodynamic and Kinetic Data for Cation Macrocycle Interaction. *Chem. Rev.* **1985**, *85*, 271-339.

(4) Allen, F. H. The Cambridge Structural Database: A Quarter of a Million Crystal Structures and Rising. *Acta Crystallogr. Sect. B: Struct. Sci.* **2002**, *58*, 380-388.

(5) Shubert, V. A.; James, W. H.; Zwier, T. S. Jet-Cooled Electronic and Vibrational Spectroscopy of Crown Ethers: Benzo-15-Crown-5 Ether and 4'-Amino-Benzo-15-Crown-5 Ether. *J. Phys. Chem. A* **2009**, *113*, 8055-8066.

(6) Shubert, V. A.; Muller, C. W.; Zwier, T. S. Water's Role in Reshaping a Macrocycle's Binding Pocket: Infrared and Ultraviolet Spectroscopy of Benzo-15-Crown-5-$(H_2O)_n$ and 4 '-Aminobenzo-15-Crown-5-$(H_2O)_n$, n=1, 2. *J. Phys. Chem. A* **2009**, *113*, 8067-8079.

(7) Kusaka, R.; Inokuchi, Y.; Ebata, T. Laser Spectroscopic Study on the Conformations and the Hydrated Structures of Benzo-18-Crown-6-Ether and Dibenzo-18-Crown-6-Ether in Supersonic Jets. *Phys. Chem. Chem. Phys.* **2007**, *9*, 4452-4459.

(8) Kusaka, R.; Inokuchi, Y.; Ebata, T. Structure of Hydrated Clusters of Dibenzo-18-Crown-6-Ether in a Supersonic Jet-Encapsulation of Water Molecules in the Crown Cavity. *Phys. Chem. Chem. Phys.* **2008**, *10*, 6238-6244.

(9) Kusaka, R.; Inokuchi, Y.; Ebata, T. Water-Mediated Conformer Optimization in Benzo-18-Crown-6-Ether/Water System. *Phys. Chem. Chem. Phys.* **2009**, *11*, 9132-9140.

(10) Kokubu, S.; Kusaka, R.; Inokuchi, Y.; Haino, T.; Ebata, T. Laser Spectroscopic Study on (Dibenzo-24-Crown-8-Ether)-Water and -Methanol Complexes in Supersonic Jets. *Phys. Chem. Chem. Phys.* **2010**, *12*, 3559-3565.

(11) Kusaka, R.; Kokubu, S.; Inokuchi, Y.; Haino, T.; Ebata, T. Structure of Host-Guest Complexes between Dibenzo-18-Crown-6 and Water, Ammonia, Methanol, and Acetylene: Evidence of Molecular Recognition on the Complexation. *Phys. Chem. Chem. Phys.* **2011**, *13*, 6827-6836.

(12) Inokuchi, Y.; Kusaka, R.; Ebata, T.; Boyarkin, O. V.; Rizzo, T. R. Laser Spectroscopic Study of Cold Host-Guest Complexes of Crown Ethers in the Gas Phase. *ChemPhysChem* **2013**, *14*, 649-660.

(13) Kusaka, R.; Inokuchi, Y.; Haino, T.; Ebata, T. Structures of (3*n*-Crown-*n*)-Phenol (n = 4, 5, 6, 8) Host-Guest Complexes: Formation of a Uniquely Stable Complex for n = 6 Via Collective Intermolecular Interaction. *J. Phys. Chem. Lett.* **2012**, *3*, 1414-1420.

(14) Morishima, F.; Kusaka, R.; Inokuchi, Y.; Haino, T.; Ebata, T. Anomalous Cage Effect of the Excited State Dynamics of Catechol in the 18-Crown-6-Catechol Host-Guest Complex. *J. Phys. Chem. B* **2015**, *119*, 2557-2565.

(15) Choi, C. M.; Kim, H. J.; Lee, J. H.; Shin, W. J.; Yoon, T. O.; Kim, N. J.; Heo, J. Ultraviolet Photodepletion Spectroscopy of Dibenzo-18-Crown-6-Ether Complexes with Alkali Metal Cations. *J. Phys. Chem. A* **2009**, *113*, 8343-8350.

(16) Choi, C. M.; Choi, D. H.; Heo, J.; Kim, N. J.; Kim, S. K. Ultraviolet–Ultraviolet Hole Burning Spectroscopy in a Quadrupole Ion Trap: Dibenzo[18]Crown-6 Complexes with Alkali Metal Cations. *Angew. Chem. Int. Ed.* **2012**, *51*, 7297-7300.
(17) Choi, C. M.; Baek, J. Y.; Park, K. S.; Heo, J.; Kim, N. J. Conformation-Specific Ultraviolet Spectroscopy of Benzo-18-Crown-6 Complexes with a Potassium Cation. *Chem. Phys. Lett.* **2014**, *593*, 150-153.
(18) Inokuchi, Y.; Boyarkin, O. V.; Kusaka, R.; Haino, T.; Ebata, T.; Rizzo, T. R. UV and IR Spectroscopic Studies of Cold Alkali Metal Ion-Crown Ether Complexes in the Gas Phase. *J. Am. Chem. Soc.* **2011**, *133*, 12256-12263.
(19) Inokuchi, Y.; Boyarkin, O. V.; Kusaka, R.; Haino, T.; Ebata, T.; Rizzo, T. R. Ion Selectivity of Crown Ethers Investigated by UV and IR Spectroscopy in a Cold Ion Trap. *J. Phys. Chem. A* **2012**, *116*, 4057-4068.
(20) Inokuchi, Y.; Ebata, T.; Rizzo, T. R.; Boyarkin, O. V. Microhydration Effects on the Encapsulation of Potassium Ion by Dibenzo-18-Crown-6. *J. Am. Chem. Soc.* **2014**, *136*, 1815-1824.
(21) Inokuchi, Y.; Ebata, T.; Rizzo, T. R. Solvent Effects on the Encapsulation of Divalent Ions by Benzo-18-Crown-6 and Benzo-15-Crown-5. *J. Phys. Chem. A* **2015**, *119*, 8097-8105.
(22) Inokuchi, Y.; Ebata, T.; Rizzo, T. R. UV and IR Spectroscopy of Cold H_2O^+-Benzo-Crown Ether Complexes. *J. Phys. Chem. A* **2015**, *119*, 11113-11118.
(23) Inokuchi, Y.; Haino, T.; Sekiya, R.; Morishima, F.; Dedonder, C.; Feraud, G.; Jouvet, C.; Ebata, T. UV Photodissociation Spectroscopy of Cryogenically Cooled Gas Phase Host-Guest Complex Ions of Crown Ethers. *Phys. Chem. Chem. Phys.* **2015**, *17*, 25925-25934.
(24) Inokuchi, Y.; Nakatsuma, M.; Kida, M.; Ebata, T. Conformation of Alkali Metal Ion-Benzo-12-Crown-4 Complexes Investigated by UV Photodissociation and UV-UV Hole-Burning Spectroscopy. *J. Phys. Chem. A* **2016**, *120*, 6394-6401.
(25) Inokuchi, Y.; Soga, K.; Hirai, K.; Kida, M.; Morishima, F.; Ebata, T. Ultraviolet Photodissociation Spectroscopy of the Cold K^+.Calix[4]Arene Complex in the Gas Phase. *J. Phys. Chem. A* **2015**, *119*, 8512-8518.
(26) Kang, H.; Féraud, G.; Dedonder-Lardeux, C.; Jouvet, C. New Method for Double-Resonance Spectroscopy in a Cold Quadrupole Ion Trap and Its Application to UV–UV Hole-Burning Spectroscopy of Protonated Adenine Dimer. *J. Phys. Chem. Lett.* **2014**, *5*, 2760-2764.
(27) Kobayashi, Y.; Inokuchi, Y.; Ebata, T. Ion Core Structure in $(CS_2)_n^+$ and $(CS_2)_n^-$ (n = 3-10) Studied by Infrared Photodissociation Spectroscopy. *J. Chem. Phys.* **2008**, *128*, 164319.
(28) Goto, H.; Osawa, E. Corner Flapping: A Simple and Fast Algorithm for Exhaustive Generation of Ring Conformations. *J. Am. Chem. Soc.* **1989**, *111*, 8950-8951.
(29) Goto, H.; Osawa, E. An Efficient Algorithm for Searching Low-Energy Conformers of Cyclic and Acyclic Molecules. *J. Chem. Soc.-Perkin Trans. 2* **1993**, 187-198.
(30) Inokuchi, Y.; Ebata, T.; Ikeda, T.; Haino, T.; Kimura, T.; Guo, H.; Furutani, Y. New Insights into Metal Ion-Crown Ether Complexes Revealed by SEIRA Spectroscopy. *New J. Chem.* **2015**, *39*, 8673-8680.

(31) Frisch, M. J.; Trucks, G. W.; Schlegel, H. B.; Scuseria, G. E.; Robb, M. A.; Cheeseman, J. R.; Scalmani, G.; Barone, V.; Mennucci, B.; Petersson, G. A., et al. *Gaussian 09, Revision A.1*, Gaussian, Inc.: Wallingford CT, 2009.
(32) Schuchardt, K. L.; Didier, B. T.; Elsethagen, T.; Sun, L. S.; Gurumoorthi, V.; Chase, J.; Li, J.; Windus, T. L. Basis Set Exchange: A Community Database for Computational Sciences. *J. Chem. Inf. Model.* **2007**, *47*, 1045-1052.
(33) Inokuchi, Y.; Boyarkin, O. V.; Ebata, T.; Rizzo, T. R. UV and IR Spectroscopy of Cold 1,2-Dimethoxybenzene Complexes with Alkali Metal Ions. *Phys. Chem. Chem. Phys.* **2012**, *14*, 4457-4462.
(34) Yi, J. T.; Ribblett, J. W.; Pratt, D. W. Rotationally Resolved Electronic Spectra of 1,2-Dimethoxybenzene and the 1,2-Dimethoxybenzene-Water Complex. *J. Phys. Chem. A* **2005**, *109*, 9456-9464.
(35) Wessel, J. E.; Syage, J. A. Excitonic Interactions in Naphthalene Clusters. *J. Phys. Chem.* **1990**, *94*, 737-747.
(36) Seurre, N.; Le Barbu-Debus, K.; Lahmani, F.; Zehnacker-Rentien, A.; Sepioł, J. Electronic and Vibrational Spectroscopy of Jet-Cooled M-Cyanophenol and Its Dimer: Laser-Induced Fluorescence and Fluorescence-Dip IR Spectra in the S_0 and S_1 States. *Chem. Phys.* **2003**, *295*, 21-33.
(37) Kopec, S.; Köppel, H. Theoretical Analysis of the $S_2 \leftarrow S_0$ Vibronic Spectrum of the 2-Pyridone Dimer. *J. Chem. Phys.* **2016**, *144*, 024314.
(38) Müller, A.; Talbot, F.; Leutwyler, S. S1/S2 Exciton Splitting in the $(2\text{-Pyridone})_2$ Dimer. *J. Chem. Phys.* **2002**, *116*, 2836-2847.
(39) Ottiger, P.; Leutwyler, S.; Köppel, H. S_1/S_2 Excitonic Splittings and Vibronic Coupling in the Excited State of the Jet-Cooled 2-Aminopyridine Dimer. *J. Chem. Phys.* **2009**, *131*.
(40) Heid, C. G.; Ottiger, P.; Leist, R.; Leutwyler, S. The S_1/S_2 Exciton Interaction in 2-Pyridone•6-Methyl-2-Pyridone: Davydov Splitting, Vibronic Coupling, and Vibronic Quenching. *J. Chem. Phys.* **2011**, *135*.
(41) Ottiger, P.; Leutwyler, S. Excitonic Splittings in Jet-Cooled Molecular Dimers. *Chimia* **2011**, *65*, 228-230.
(42) Kopec, S.; Ottiger, P.; Leutwyler, S.; Köppel, H. Vibrational Quenching of Excitonic Splittings in H-Bonded Molecular Dimers: Adiabatic Description and Effective Mode Approximation. *J. Chem. Phys.* **2012**, *137*.
(43) Ottiger, P.; Leutwyler, S. Excitonic Splitting and Coherent Electronic Energy Transfer in the Gas-Phase Benzoic Acid Dimer. *J. Chem. Phys.* **2012**, *137*.
(44) Ottiger, P.; Leutwyler, S.; Köppel, H. Vibrational Quenching of Excitonic Splittings in H-Bonded Molecular Dimers: The Electronic Davydov Splittings Cannot Match Experiment. *J. Chem. Phys.* **2012**, *136*.
(45) Balmer, F. A.; Ottiger, P.; Leutwyler, S. Excitonic Splitting, Delocalization, and Vibronic Quenching in the Benzonitrile Dimer. *J. Phys. Chem. A* **2014**, *118*, 11253-11261.
(46) Kopec, S.; Ottiger, P.; Leutwyler, S.; Köppel, H. Analysis of the $S_2 <- S_0$ Vibronic Spectrum of the Ortho-Cyanophenol Dimer Using a Multimode Vibronic Coupling Approach. *J. Chem. Phys.* **2015**, *142*.
(47) Ottiger, P.; Köppel, H.; Leutwyler, S. Excitonic Splittings in Molecular Dimers: Why Static Ab Initio Calculations Cannot Match Them. *Chem. Sci.* **2015**, *6*, 6059-6068.

(48) Balmer, F. A.; Kopec, S.; Köppel, H.; Leutwyler, S. Excitonic Splitting and Vibronic Coupling Analysis of the M-Cyanophenol Dimer. *J. Phys. Chem. A* **2016**. DOI: 10.1021/acs.jpca.6b10416.

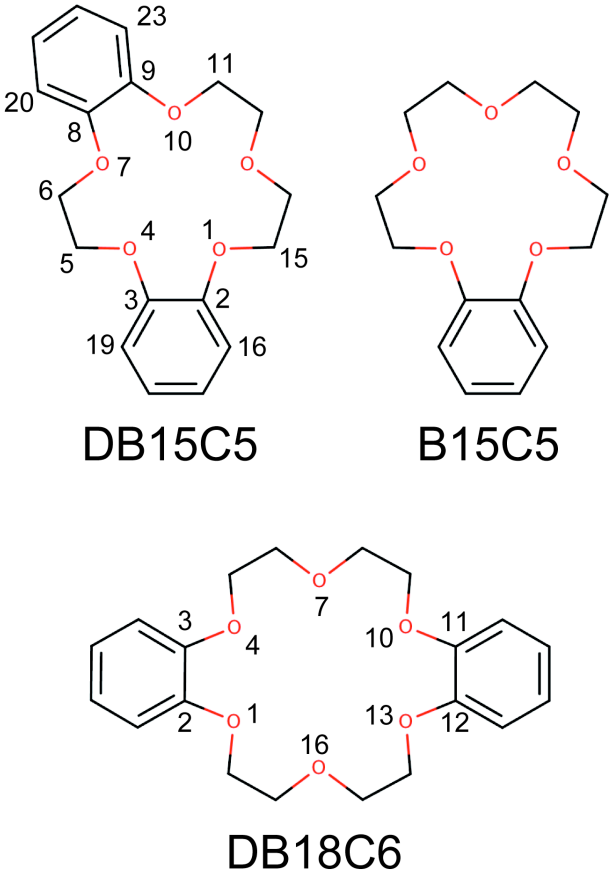
23
9
11
20
O
8
10
O 7
O
6
4
1
5
O
O
15
3
2
19
16
DB15C5
O
O
O
O
O
O
B15C5
O
7
3
O
4
10
O
11
2
O
1
13
O
12
16
O
DB18C6

Scheme 1.

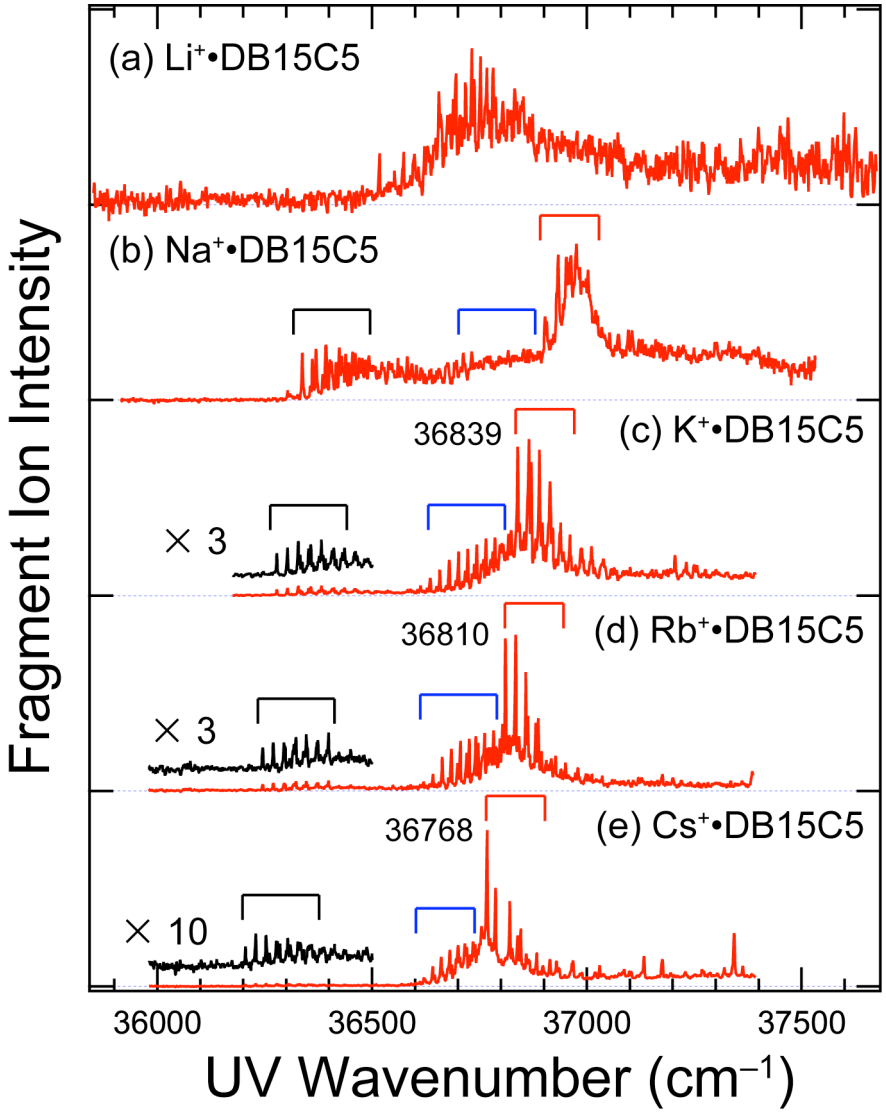

Figure 1. UVPD spectra of the M^+•DB15C5 (M = Li, Na, K, Rb, and Cs) complexes.

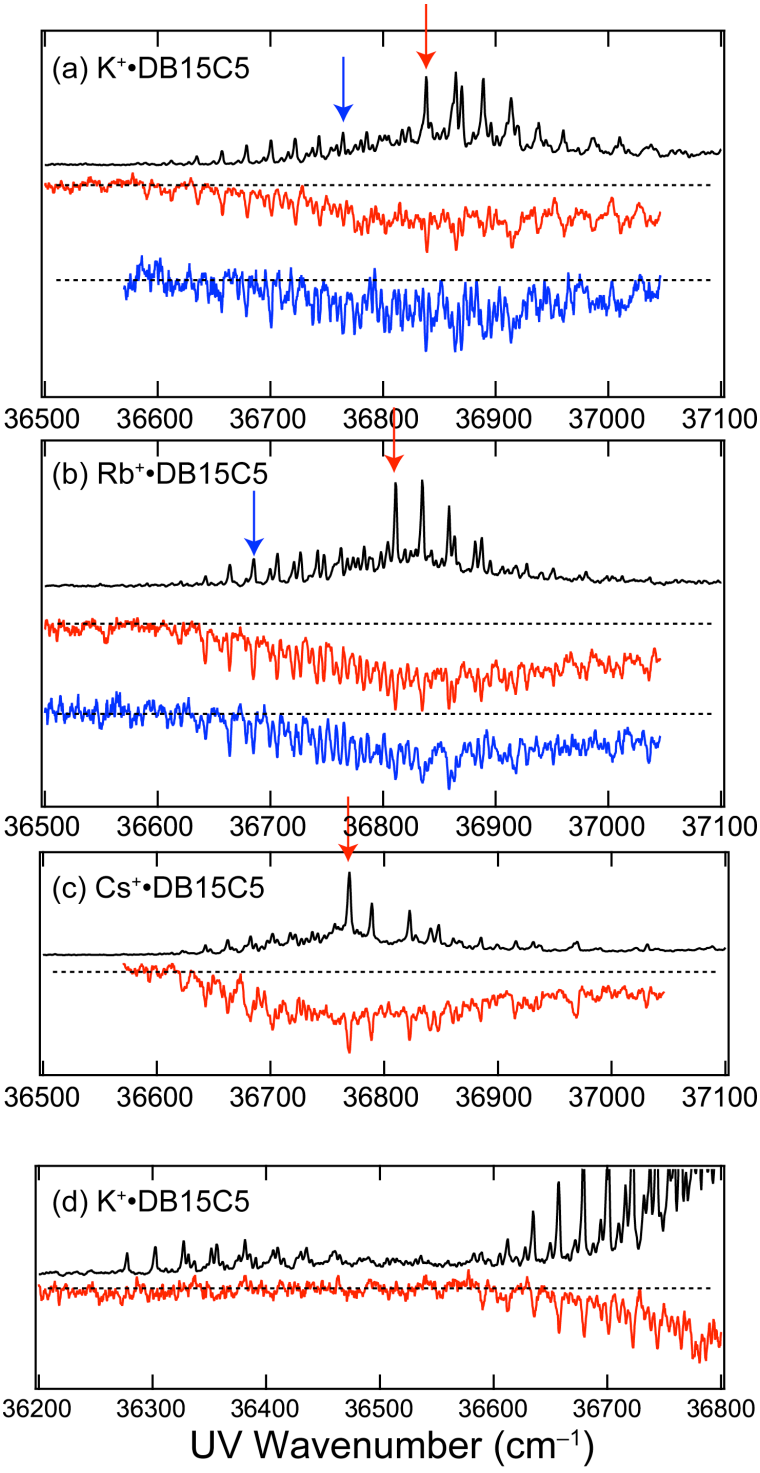

Figure 2. UV-UV HB spectra (red and blue) and the UVPD spectra (black) of the M^+•DB15C5 (M = K, Rb, and Cs) complexes. The positions of the probe laser are shown with arrows in the UVPD spectra.

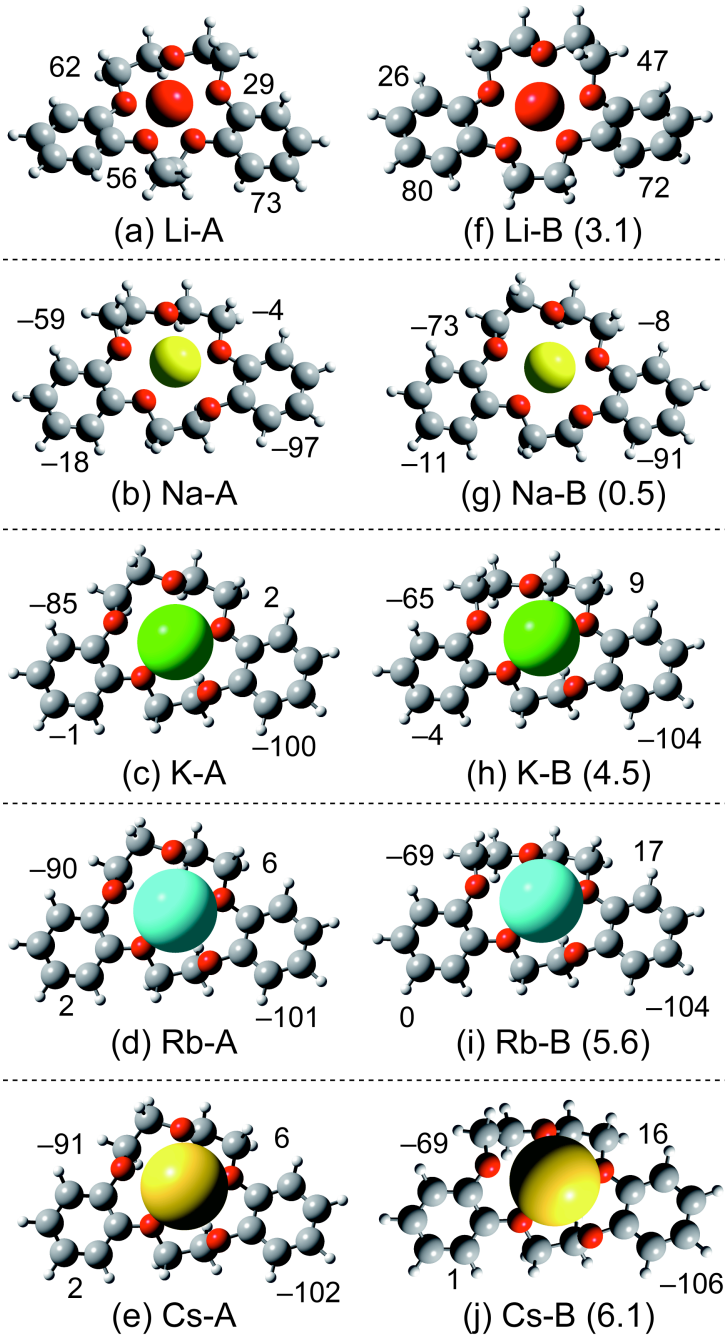

Figure 3. Optimized structures of the M^+•DB15C5 (M = Li, Na, K, Rb, and Cs) complexes. The numbers in the figure present the dihedral angles of C15–O1–C2–C16, C5–O4–C3–C19, C6–O7–C8–C20, and C11–O10–C9–C23 (see Scheme 1) in degrees. The numbers in parentheses show the total energy relative to that of the most stable conformers (Li-A, Na-A, K-A, Rb-A, and Cs-A) in kJ/mol. It should be noted that conformers Na-B, K-A, Rb-A, and Cs-A have similar structures to each other. Conformers Na-A, K-B, Rb-B, and Cs-B also have similar forms to each other.

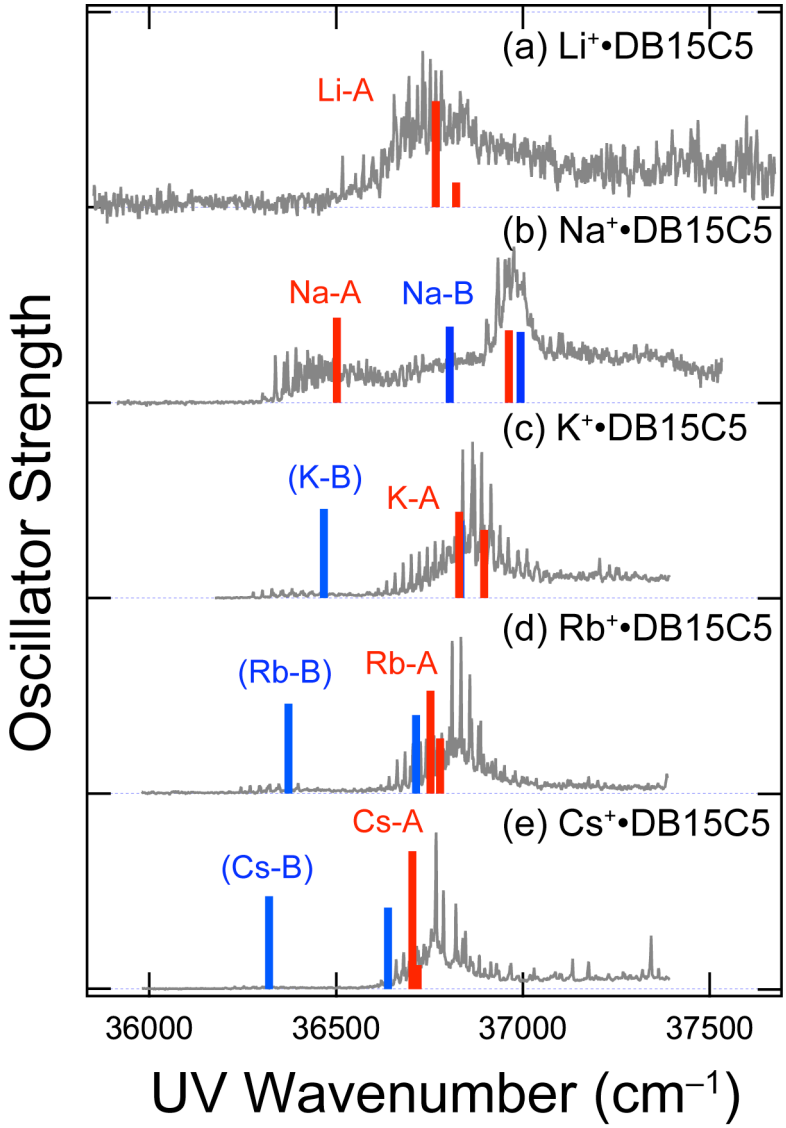

Figure 4. Comparison of the UVPD spectra and the results of TD-DFT calculations (red and blue bars). A scaling factor of 0.8340 is employed for the calculated transition energy. This factor was determined for the K^+•DB18C6 complex in our previous paper (Ref. 18).

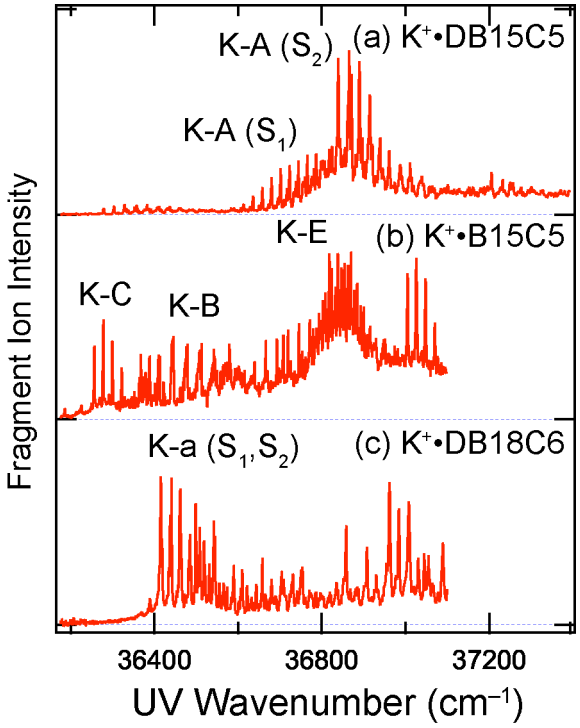

Figure 5. The UVPD spectra of (a) K^+•DB15C5, (b) K^+•B15C5, and (c) K^+•DB18C6 complexes. The spectra in Figs. 5b and c are taken from our previous papers (Refs. 19 and 18).

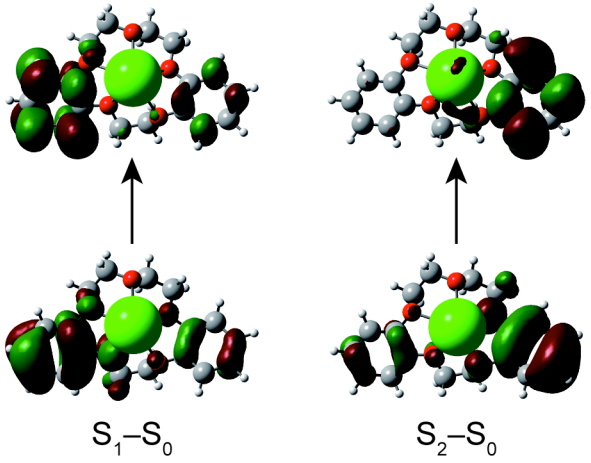

Figure 6. Molecular orbitals that contribute the most to the S_1–S_0 and S_2–S_0 transitions of (a) K^+•DB15C5 and (b) K^+•DB18C6 (Ref. 18).

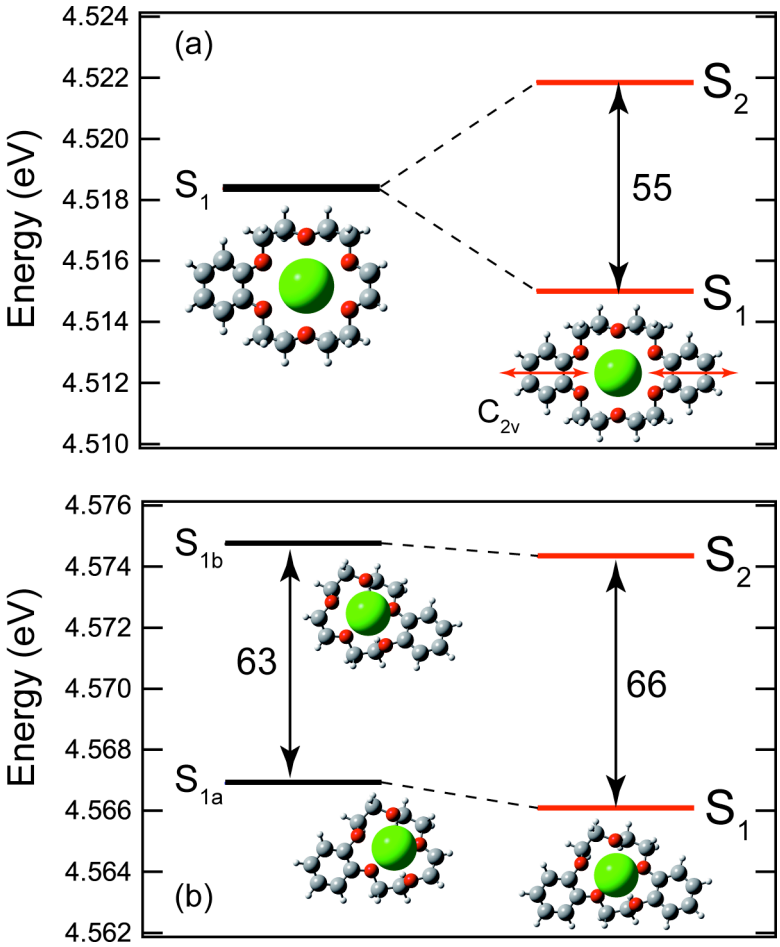

Figure 7. Energy levels of the electronic excited states of the two chromophores and the complexes for (a) K^+•DB18C6 and (b) K^+•DB15C5. The vertical axis is the energy with respect to the electronic ground state of each species. The structures in the figure are the K^+ complexes used for the calculation of the UV transition energy of the two chromophores and the complexes. The scaling factor of 0.8340 is employed also for the calculated energy in this figure. The numbers in the figure show the energy difference in cm^{-1}. The red arrows in part a show the direction of the transition dipole moment of the two chromphores.

Table 1. Number of conformers found experimentally for the M^+•DB15C5, M^+•B15C5, and M^+•DB18C6 (M = Li, Na, K, Rb, and Cs) complexes under the cold conditions.

M	M^+•DB15C5	M^+•B15C5[a]	M^+•DB18C6[b]
Li	1	2	2
Na	2	1	2
K	1	3	1
Rb	1	3	1
Cs	1	3	1

[a]Ref. 19.
[b]Ref. 18.

Table 2. Transition dipole moments, distance of benzene rings, and estimated exciton splitting energies for the K^+•DB15C5 and K^+•DB18C6 complexes.

	$\lvert\mu_a\rvert$ (10^{-30} Cm)	$\lvert\mu_b\rvert$ (10^{-30} Cm)	R_{ab} (Å)	$\lvert\mu_a\rvert\lvert\mu_b\rvert/4\pi\varepsilon_0 R_{ab}^3$ (cm^{-1})	$V_{ab}{}^a$ (cm^{-1})	$V_{ab}{}^b$ (cm^{-1})
K^+•DB18C6	5.6	5.6	9.1	18	33	27
K^+•DB15C5	4.4	4.5	8.0	17	17	10

[a]Calculated with equation (3).
[b]Estimated with the results of the TD-DFT calculations shown in Fig. 7.

Table 3. Contribution (%) of the electronic transition of two chromophores (benzene a and b) to the S_1–S_0 and S_2–S_0 transition of the K^+•DB15C5 complex.

	conformer	transition	contribution (%)[a]		contribution (%)[b]	
			benzene a	benzene b	benzene a	benzene b
K^+•DB15C5	K-A	S_1–S_0	97	3	72	0
		S_2–S_0	3	97	3	67

[a]Calculated on the basis of the S_1–S_0 and S_2–S_0 transition energies of the complexes and the S_1–S_0 transition energy of two chromophores.
[b]Estimated from the results of the TD-DFT calculations (coefficients for electron promotion between two MOs).

TOC figure